Proc. Instn Civ. Engrs Wat., Marit. & Energy, 1995, **112**, Mar., 20–30

Water Board Water Panel Paper 10339

Written discussion closes 15 May 1995

Predicting oxygen content downstream of weirs, spillways and waterways

EurIng H. Chanson, ME, PhD, MIEAust, IAHR

At hydraulic structures (e.g. weirs, spillways), air-water transfer of atmospheric gases (e.g. oxygen) occurs by self-aeration along the chute and by flow aeration in the hydraulic jump at the downstream end of the structure. In this Paper, experimental data are re-analysed and compared with a numerical method to predict the free-surface aeration. Aeration at hydraulic jumps is also examined and compared with existing correlations. Calculations of free-surface aeration and empirical correlations for hydraulic jump aeration are combined to predict the dissolved oxygen content downstream of weirs and spillways. Good agreement between calculations and prototype data is obtained. The results indicate that self-aeration might contribute to a large part of the oxygenation taking place at hydraulic structures for small water discharges. For large discharges, the reduction or the disappearance of free-surface aeration affects substantially the aeration efficiency.

Notation

A water quality coefficient
a specific air-water interface area (m^{-1})
a_{mean} mean specific interface area (m^{-1}):

$$a_{mean} = \frac{1}{Y_{90}} \int_0^{Y_{90}} a \, dy$$

B weir aeration factor
B' integration constant
C air concentration (i.e. void fraction)
C_b air concentration at the outer edge of the air concentration boundary layer
C_{DS} concentration of dissolved gas in water (kg/m^3) downstream of hydraulic structure
C_{gas} concentration of dissolved gas in water (kg/m^3)
C_{mean} depth averaged air concentration: $(1-Y_{90})$ $C_{mean} = d$
C_s gas saturation concentration in water (kg/m^3)
C_{US} concentration of dissolved gas in water (kg/m^3) upstream of hydraulic structure
D_{gas} molecular diffusivity of gas in water (m^2/s)
d mean water flow depth (m): $d = \int_0^{Y_{90}} (1 - C)\, dy$
d_b air bubble diameter (m)
d_m maximum air bubble diameter (m)
d_p water droplet diameter (m)
d_T transition depth (m) defined as the depth where dC/dy is maximum
$(d_b)_c$ maximum bubble size (m) in turbulent shear flow
E aeration efficiency
E_{HJ} aeration efficiency of hydraulic jump
E_{SA} aeration efficiency due to self-aeration
Fr Froude number
G' integration constant
g gravity constant (m/s^2)
K_L liquid film coefficient (m/s)
k_s roughness height (m)
$L_{spillway}$ spillway length (m)
q discharge per unit width (m^2/s)
$(q_w)_c$ critical discharge (m^2/s)
Re Reynolds number
r deficit ratio
T temperature (Kelvin)
t time (s)
U_w average flow velocity (m/s): $U_w = q_w/d$
V velocity (m/s)
V_{90} characteristic velocity (m/s) at which $y = Y_{90}$
v'^2 spatial average value of the square of the velocity differences over a distance equal to d_b
W channel width (m)
$(We)_c$ critical Weber number:

$$(We)_c = \frac{\rho_w v'^2 (d_b)_c}{2\sigma}$$

$(We)_e$ self-aerated flow Weber number:

$$(We)_e = \rho_w \frac{V_{90}^2 Y_{90}}{\sigma}$$

x distance measured along the spillway surface (m)
Y_{60} characteristic depth (m) where $C = 60\%$
Y_{90} characteristic depth (m) where $C = 90\%$
y distance measured perpendicular to the spillway surface (m)
y' dimensionless distance: $y' = y/Y_{90}$
α spillway slope
χ factor (close to unity) varying with the air–water interface area distribution and the dissolved gas concentration distribution
δ_{ab} air concentration boundary layer thickness (m)
μ dynamic viscosity ($N\,s/m^2$)
ν kinematic viscosity (m^2/s)
ρ density (kg/m^3)
σ surface tension between air and water (N/m)
ω vorticity (s^{-1})

Subscript
w water flow

Introduction

Presentation

One of the most important water quality parameters in rivers and streams is dissolved oxygen (DO). The oxygen concentration is a prime indicator of the quality of the water. Dams and weirs across a stream affect the air–

H. Chanson, Lecturer in Fluid Mechanics, Hydraulics and Environmental Engineering, Department of Civil Engineering, The University of Queensland, Brisbane, Australia

water gas transfer dynamics. Deep and slow pools of water upstream of a dam reduce the gas transfer process and the natural re-aeration as compared with an open river; but some hydraulic structures (e.g. spillway, stilling basin) can enhance the oxygen transfer during water releases. A typical weir structure includes a spillway followed by a dissipation basin with a hydraulic jump (Figs 1 and 2). Aeration occurs along the spillway and at the hydraulic jump in the stilling basin.

2. Previous papers (Table 1) have attempted to correlate the oxygen transfer at hydraulic structures. Most studies provide empirical correlations to estimate the overall transfer efficiency, but the application of such correlations to a new structure is somewhat uncertain. In this article a method to predict the gas transfer caused by self-aeration is developed. The results are compared with experimental data.[1] The aeration calculations at hydraulic jumps are discussed and existing correlations are compared with prototype data. Self-aeration and hydraulic jump calculations are combined to predict the DO content downstream of weirs and spillways. The results are compared with prototype data.[1,2]

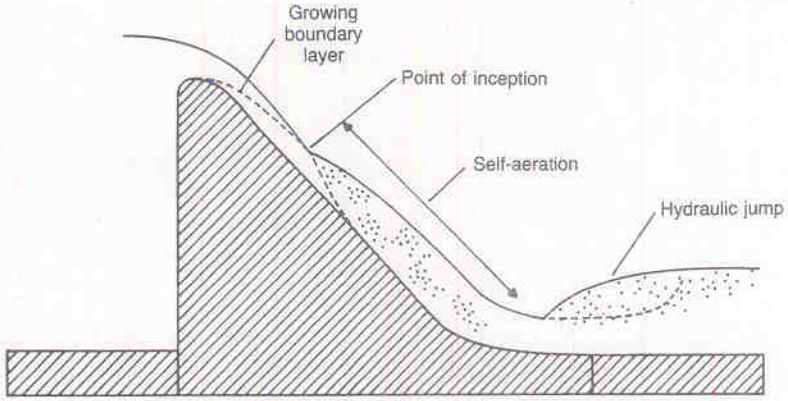

Fig. 1. Flow aeration at weirs and spillways

Air–water gas transfer

3. Fick's law states that the mass transfer rate of a chemical across an interface and in a

*Table 1. Oxygenation formula for hydraulic structures**

Reference (1)	Formula (2)	Remarks (3)
Gameson[7]	$r-1=0{\cdot}5\,A\,B\,H$ $A = 0{\cdot}85$ (sewage effluent), 1·0 (moderately polluted), 1·25 (slightly polluted) $B = 0{\cdot}2$ (slope), 1·0 (weir), 1·3 (step weir)	Model weirs
Gameson *et al.*[27]	$r-1=0{\cdot}36\,A\,B\,H\,(1+0{\cdot}046\,(T-273{\cdot}15))$	Model weirs
Holler[38]	$r_{20}-1=0{\cdot}211\,H$	Prototype weir structures: $3{\cdot}6 < H < 10{\cdot}7$ m
Department of the Environment[28]	$r-1=0{\cdot}38\,A\,B\,H\,(1-0{\cdot}11v)\,(1+0{\cdot}046\,(T-273{\cdot}15))$	
Foree[39]	$r_{25}=\exp(0{\cdot}525\,H)$	Low-level in-stream dams behaving as waterfalls
Avery and Novak[40]	$r-1=k\,Fr^{k'}\,Re^{k''}$	Weirs and hydraulic jumps
Butts and Evans[2]	Department of the Environment[28]	Prototype hydraulic structures: $0{\cdot}54 < B < 2{\cdot}20$
Nakasone[41]	$\mathrm{Ln}(r)=k\,H^{k'}\,q_w^{k''}\,d_{D/S}^{k'''}$	Weirs
Railsback *et al.*[42]	$r=\dfrac{1}{k-[k'/(C_s-C_{U/S})]}$	Navigation dams
Rindels and Gulliver[43]	$r_{20}=\exp\left(\dfrac{0{\cdot}262\,H}{1+2{\cdot}153\,q_w}+2{\cdot}034\,d_{D/S}\right)$	Prototype weirs and spillways

* A water quality coefficient[7]
B weir aeration factor
C_S saturation concentration of dissolved oxygen in water (kg/m³)
$C_{U/S}$ upstream dissolved oxygen concentration (kg/m³)
$d_{D/S}$ tailwater depth (m)
Fr Froude number
H dam height (m)
Re Reynolds number
r_{20}, r_{25} oxygen deficit ratio at 20°C, 25°C

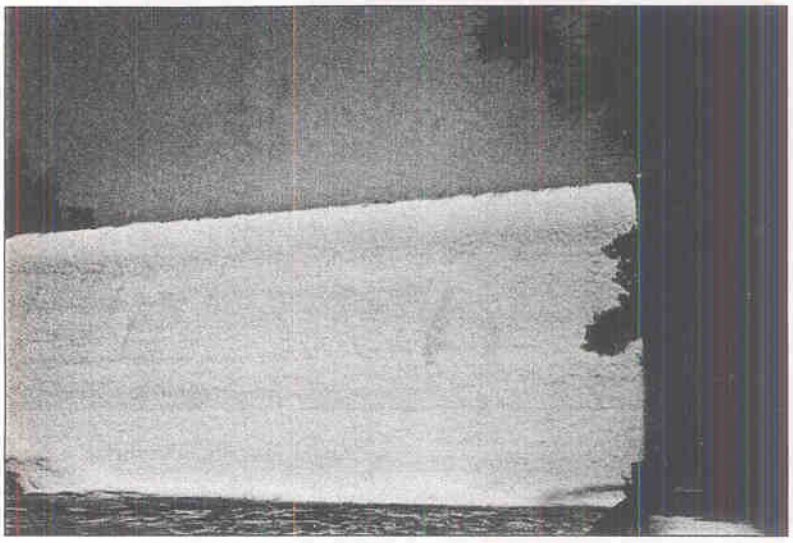

(a)

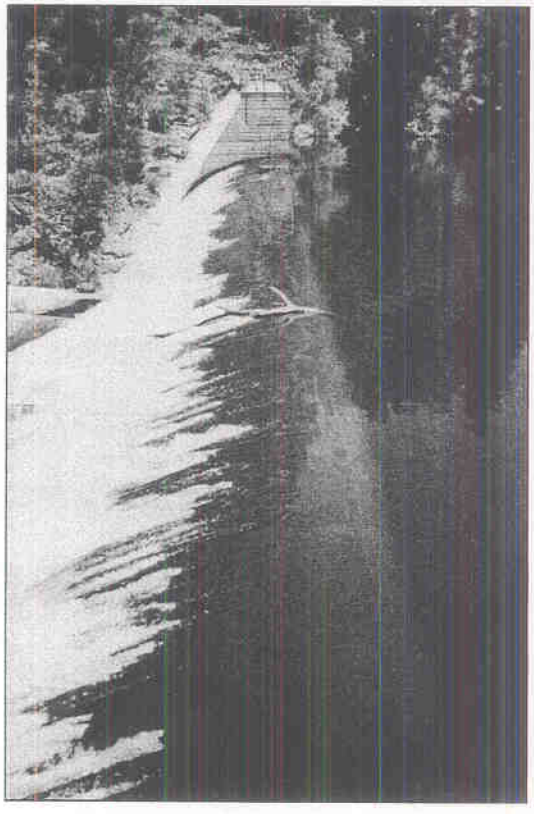

(b)

Fig. 2. Example of self-aeration—Cotter Dam, Australia (built in 1910, 27 m high): (a) view from downstram; (b) view of crest (water flows from right to left; location of inception point of air entrainment should be noted) (photographs courtesy of Mr P. D. Cummings)

quiescent fluid varies directly as the coefficient of molecular diffusion and the negative gradient of gas concentration.[3] The gas transfer of a dissolved gas (e.g. oxygen) across an air–water interface is controlled by the liquid. Using Henry's law, it is usual to write Fick's law as

$$\frac{d}{dt} C_{gas} = K_L a (C_s - C_{gas}) \quad (1)$$

where C_{gas} is the concentration of the dissolved gas in water, K_L is the liquid film coefficient, a is the specific surface area, and C_s is the gas saturation concentration of dissolved gas in water. A recent review of the transfer coefficient calculations in turbulent flows showed that K_L is almost constant regardless of the bubble size and flow situations.[4] Using Higbie's[5] penetration theory, the transfer coefficient of large bubbles (i.e. $d_b > 0{\cdot}25$ mm) affected by surface active impurities can be estimated as[4]

$$K_L = 0{\cdot}47 \sqrt{(D_{gas})} \left(\frac{\mu_w}{\rho_w}\right)^{-1/6} \sqrt[3]{g} \quad (2)$$

where D_{gas} is the molecular diffusivity, and μ_w and ρ_w are the dynamic viscosity and density of the liquid. Equation (2) was successfully compared with more than a dozen experimental studies.

4. *Application to open channel flow.* In free-surface flows along a spillway, the pressure variations are small, and the liquid density and viscosity can be assumed functions of the temperature only. In most practical applications, the temperature and salinity are constant along a chute, and the coefficient of transfer K_L and the saturation concentration C_s become two constants in equation (1). Along a channel and at each location, equation (1) can be averaged over the cross-section, and it yields[6]

$$\frac{d}{dx} C_{gas} = \frac{K_L a_{mean}}{U_w} (C_s - \chi C_{gas}) \quad (3)$$

where U_w is the mean flow velocity, a_{mean} is the mean specific interface area, and χ is a factor (close to unity) varying with the distributions of air–water interface area and dissolved gas concentration.

5. If equation (3) is integrated along a channel, flow aeration at weirs and spillways can be measured by the deficit ratio r defined as[7]

$$r = \frac{C_s - C_{US}}{C_s - C_{DS}} \quad (4)$$

where C_{US} is the upstream dissolved gas concentration, and C_{DS} is the dissolved gas concentration at the downstream end of the channel. Another measure of aeration is the aeration efficiency E as[7]

$$E = \frac{C_{DS} - C_{US}}{C_s - C_{US}} = 1 - \frac{1}{r} \quad (5)$$

6. *Effects of temperature.* The temperature effect on the flow aeration was examined by several researchers (Table 2). Reference 8 suggests the use of an exponential relation to describe the temperature dependence on oxygen transfer

$$\frac{\text{Ln}(r)}{\text{Ln}(r_{T_o})} = 1{\cdot}0241^{(T - T_o)} \quad (6)$$

*Table 2. Temperature dependence of flow aeration**

References (1)	Temperature dependence (2)	Comments (3)
Gameson *et al.*[27]	$\frac{\text{Ln}(r_T)}{\text{Ln}(r_{15})} = 1 + 0{\cdot}027\ (T - 288{\cdot}15)$	$273{\cdot}15 < T < 313{\cdot}15K$
Elmore and West[9]	$\frac{\text{Ln}(r_T)}{\text{Ln}(r_{20})} = 1{\cdot}0241^{(T-293{\cdot}15)}$	$278{\cdot}15 < T < 303{\cdot}15K$ Adopted by APHA[8]
Holler[38]	$\frac{\text{Ln}(r_T)}{\text{Ln}(r_{T_0})} = \theta^{(T-T_0)}$	θ in the range 1·014–1·047
Daniil and Gulliver[44]	$\frac{\text{Ln}(r_T)}{\text{Ln}(r_{20})} = \sqrt{\left[\left(\frac{T}{293}\right)\right]\left(\frac{\nu_{20}}{\nu}\right)\sqrt{\frac{\rho_{20}}{\rho}}}$	$273{\cdot}15 < T < 313{\cdot}15K$
Gulliver *et al.*[22]	$\frac{\text{Ln}(r_T)}{\text{Ln}(r_{T_0})} = \sqrt{\left[\left(\frac{T}{T_0}\right)\right]\left(\frac{\mu_{T_0}}{\mu_T}\right)^{3/4}\left(\frac{\rho_{T_0}}{\rho_T}\right)^{17/20}\left(\frac{\sigma_{T_0}}{\sigma_T}\right)^{3/5}}$	$273{\cdot}15 < T < 313{\cdot}15K$
Daniil *et al.*[45]	$\frac{\text{Ln}(r_T)}{\text{Ln}(r_{20})} = 1 + 0{\cdot}02103\ (T - 273{\cdot}15) + 8{\cdot}261E - 5\ (T - 273{\cdot}15)^2$	

* T_0 reference temperature
r_{15} deficit ratio at 20°C
r_{20}, ν_{20}, ρ_{22} deficit ratio, kinematic viscosity and density at 20°C

where r is the deficit ratio at temperature T, T_0 is a reference temperature, and the constant 1·0241 was obtained by reference 9.

Oxygen transfer caused by free-surface aeration

Flow description

7. Supercritical turbulent flows in open channels are characterized by large quantities of air entrained across the free-surface* (Fig. 2). The entrainment of air bubbles modifies the flow characteristics.[10,11] Further, the high level of turbulence and the air entrainment process enhance the air–water transfer of atmospheric gases and modify the downstream water quality.

8. At a spillway intake, a flow over the channel is quasi-uniform. Next to the invert, turbulence is generated and a turbulent boundary layer develops (Fig. 1). When the outer edge of the boundary layer reaches the free surface, turbulence can initiate free surface aeration. The location of the start of air entrainment is called the point of inception. Its characteristics can be computed using boundary layer methods.[10,12] Downstream of the inception point, a mixture of air and water extends gradually through the fluid. The flow characteristics can be computed using the method developed by reference 10 and extended by the Author.[11,13]

* Natural free surface aeration occurring at the water surface of high velocity flows is referred to as self-aeration.

Hydraulic characteristics of self-aerated flows

9. In self-aerated flows, the air concentration distribution can be represented by a diffusion model of the air bubbles within the air–water mixture[14] that gives the shape of the air concentration distribution for all mean air concentrations

$$C = \frac{B'}{B' + \exp(-G' \cos\alpha\ y'^2)} \qquad (7)$$

where C is the local air concentration defined as the volume of undissolved air per unit volume of air and water, B' and G' are functions of the mean air concentration only,[10,11] α is the spillway slope, $y' = y/Y_{90}$, y is the distance measured perpendicular to the invert, and Y_{90} is the depth where the air concentration is 90%.

10. Next to the invert, prototype[15] and model data[16] depart from equation (7), indicating that the air concentration tends to zero at the bottom.[13,17] A re-analysis of these data shows consistently the presence of an air concentration boundary layer in which the air concentration distribution is

$$\frac{C}{C_b} = \sqrt[3]{\frac{y}{\delta_{ab}}} \qquad (8)$$

where C_b is the air concentration at the outer edge of the air concentration boundary layer, and δ_{ab} is the air concentration boundary layer thickness. On Aviemore spillway, the Author[13,17] estimated $\delta_{ab} = 15$ mm. C_b satisfies the continuity between equations (7) and (8). For spillway flows, the characteristic depth Y_{90} is much larger than δ_{ab} and a reasonable approximation is: $C_b \sim B'/(1 + B')$.

Table 3. Critical Weber numbers for the splitting of air bubbles in water flows

Reference (1)	$(We)_c$ (2)	Fluid (3)	Flow situation (4)	Comments (5)
Hinse[18]	0·585		Two co-axial cylinders, the inner one rotating	Dimensional analysis
Sevik and Park[30]	1·26	Air bubbles in water	Circular water jet discharging vertically	Experimental data. V in the range 2·1–4·9 m/s
Killen[46]	1·017	Air bubbles in water	Turbulent boundary layer	Experimental data. V in the range 3·66–18·3 m/s
Lewis and Davidson[33]	2·35	Air and helium bubbles in water and fluorisol	Circular jet discharging vertically	Experimental data. V in the range 0·9–2·2 m/s
Evans *et al.*[32]	0·60	Air bubbles in water	Confined plunging water jet	Experimental data. V in the range 7·8–15 m/s Note: measurements of bubble size outside jet mixing zone
Lewis and Davidson[33]	2·35	Cylindrical bubble surrounded by inviscid liquid	Axi-symmetric shear flow	Theoretical value

11. Velocity measurements in self-aerated flows, performed on model[16] and prototype,[15] showed that the velocity distribution follows a 1/6 power law distribution

$$\frac{V}{V_{90}} = \left(\frac{y}{Y_{90}}\right)^{1/6} \tag{9}$$

and is independent of the mean air concentration. For a given mean air concentration, the characteristic velocity V_{90} is deduced from the continuity equation for the water flow[11]

$$\frac{V_{90}}{U_w} = (1 - C_{mean}) \left(\int_0^1 (1 - C)\, y'^{1/6}\, dy' \right)^{-1}$$

where C is computed using equations (7) and (8).

Air–water interface area

12. In a turbulent shear flow, the maximum air bubble size is determined by the balance between the capillary force and the inertial force caused by the velocity change over distances of the order of the bubble diameter. The splitting of air bubbles in water occurs for[18]

$$\frac{\rho_w v'^2\, d_b}{2\sigma} > (We)_c \tag{10}$$

where σ is the surface tension between air and water, d_b is the bubble diameter, and v'^2 is the spatial average value of the square of the velocity differences over a distance equal to d_b. Experiments showed that the critical Weber number $(We)_c$ is a constant near unity (Table 3). Assuming that the air bubble diameter is of the order of magnitude of the Prandtl mixing length (see Appendix 1), a maximum bubble size in self-aerated flows $(d_b)_c$ is deduced from equation (10)

$$\frac{(d_b)_c}{Y_{90}} \sim \sqrt[3]{\left[72\, \frac{(We)_c}{(We)_e} \left(\frac{y}{Y_{90}}\right)^{5/3} \right]} \tag{11}$$

where $(We)_e$ is the self-aerated flow Weber number: $(We)_e = \rho_w V_{90}^2\, Y_{90}/\sigma$.

13. With the hypothesis that: {H1} the critical Weber number equals unity, and {H2} the bubble diameter is of the order of magnitude of the mixing length, equation (11) is compared in Fig. 3 with experimental data obtained from prototypes and models. The good agreement between experiments and calculations (equation (11)) suggests that the assumptions {H1} and {H2} are reasonable, and that equation (11) provides an estimate of the maximum bubble size in self-aerated flows.

14. High speed photographs[19,20] showed that the shape of air bubbles in self-aerated flows is approximately spherical and the specific interface area equals

$$a = 6\, \frac{C}{d_b} \tag{12a}$$

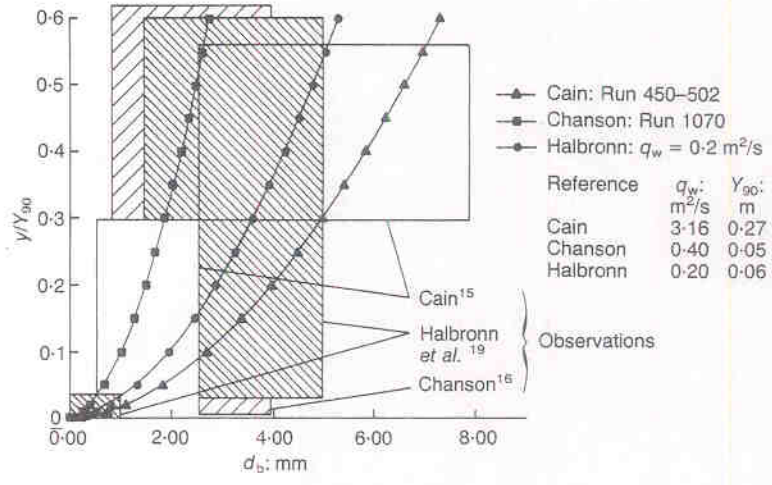

Fig. 3. Bubble size distribution in self-aerated flows: comparison between equation (11) and experimental data

for air bubbles in water. For water droplets in air, the interface area is

$$a = 6\,\frac{1-C}{d_p} \qquad (12b)$$

where d_p is the diameter of the water particles.

15. The calculation of the air–water interface requires the definition of an 'ideal' air–water interface. An advantageous choice is the location where the air concentration is 50%. This definition is consistent with experimental observations (Appendix 2) and satisfies the continuity of equation (12).

16. Equations (11) and (12) enable the calculation of the air–water surface area in the air-in-water flow. Little information is available on the size of the water droplets surrounded by water. Photographs suggest that the droplet sizes are of similar size as the large air bubbles,[21] and equation (11) may provide a first estimate of the droplet sizes. It must be emphasized that the contribution of large particles (bubbles or droplets) to the interface area is relatively small.

17. In Fig. 4, equations (7), (8), (9), (11) and (12) are plotted and compared with air concentration and velocity data obtained on Aviemore spillway.[15]

Application: aeration efficiency of chutes

18. For spillway flows, the characteristics of the point of inception can be computed using Wood's formula.[10] Downstream of the inception point (Fig. 1), the aerated flow characteristics can be computed using a simple numerical model.[11,16] The results validating the model were presented elsewhere.[11] The Author[6] showed that the air–water gas transfer resulting from self-aeration can be estimated at any position along a spillway.

19. Rindels and Gulliver[1] reported several measurements of DO content upstream, downstream and along spillways and weirs. Their photographs show clearly the existence of 'white waters' (i.e. free-surface aeration). For these measurements, the self-aeration efficiencies are deduced from the upstream DO content and the DO content at various positions along the chute upstream of the hydraulic jump. These data are compared with self-aeration predictions in Fig. 5. Fig. 5 shows a reasonable agreement between the prediction and the measurements.

Discussion: Mean specific interface area

20. Dimensional analysis[6] indicates that the mean specific interface area is a function of the self-aerated flow parameters (Y_{90}, V_{90}, C_{mean}) and the fluid properties (ρ_w, σ)

$$a_{mean}\,Y_{90} = f_1\left(C_{mean};\ \frac{\delta_{ab}}{Y_{90}};\ (We)_e\right) \qquad (13)$$

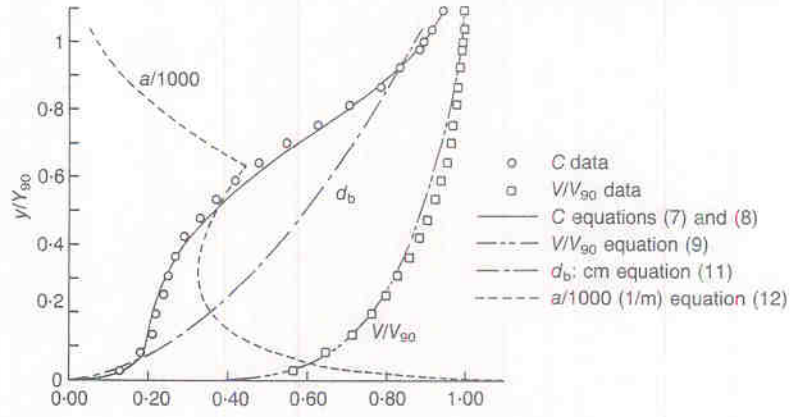

Fig. 4. Air concentration, velocity, bubble size and specific air–water interface area distributions on Aviemore spillway:[15] *$q_w = 2{\cdot}23\ m^2/s$; $Y_{90} = 0{\cdot}22\ m$*

21. The Author investigated the effects of the mean air concentration and Weber number on the specific interface area using equations (7), (11) and (12). The results indicate that the interface area can be correlated as

$$a_{mean}\,Y_{90} = 4{\cdot}193\,(C_{mean})^{1{\cdot}538}\,\sqrt[3]{(We)_e} \qquad (14)$$

Equation (14) is obtained for C_{mean} between 0·05 and 0·60, and $(We)_e$ ranging from $1E+5$ up to $1E+9$ with a normalized correlation of 0·98.

22. On prototype spillways, typical values of $V_{90} = 20$ m/s and $Y_{90} = 1$ m imply $(We)_e = 5{\cdot}4\ 10^6$. For a mean air concentration $C_{mean} = 0{\cdot}30$, the mean specific area is: $a_{mean} = 101\ m^{-1}$. Gulliver *et al.*[22] re-analysed high-speed photographs obtained by Straub[20,23] of a sectional view of self-aerated flows through a glass sidewall. Their analysis of the photographs indicated at the specific area is independent of the flow depth and flow parameters, and may be estimated as

$$a_{mean} = 6{\cdot}49\,\frac{C_{mean}}{d_m} \qquad (15)$$

where d_m is the maximum bubble diameter observed ($d_m = 2{\cdot}7$ mm). Equation (15) implies $a_{mean} = 721\ m^{-1}$ for $C_{mean} = 0{\cdot}30$. The Author believes that the photographic technique used

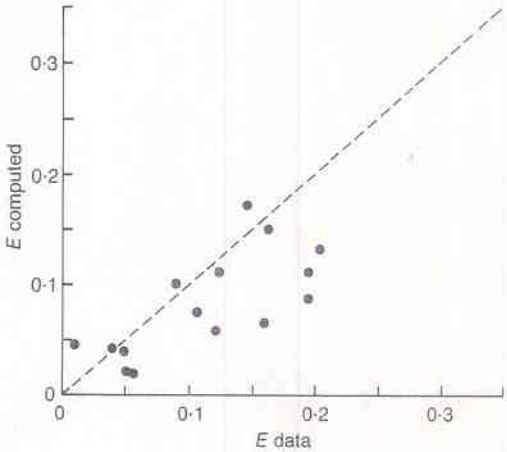

Fig. 5. Oxygen transfer resulting from free-surface aeration: comparison between correlations and experimental data[1]

by Gulliver *et al.*[22] gives the bubble size distribution in the side-wall boundary layer, which is characterized by higher shear stress and smaller bubble sizes than on the centre-line. This might explain the differences obtained for the interface areas.

Oxygen transfer at hydraulic jumps

23. At the downstream end of a spillway, most flows are supercritical and the total head is larger than that of the downstream river. Most river and stream flow regimes are subcritical: a transition from supercritical to subcritical (i.e. hydraulic jump) occurs near the end of the spillway (Fig. 1). The hydraulic jump is characterized by the development of large-scale turbulence, energy dissipation and air entrainment. Gas transfer results from the large number of entrained air bubbles and the turbulent mixing in the jump. Several researchers have proposed correlations to predict the oxygen transfer (Table 4). Johnson[24] developed an empirical fit of prototype data that works well with relatively deep plunge pools. However, Rindels and Gulliver[25] showed that Johnson's method does not apply to the re-aeration of low DO contents with shallow plunge pools.

24. The Author re-analysed field data[1] which provided DO measurements immediately upstream and downstream of hydraulic jumps. The upstream flow conditions of the jump were computed from growing boundary layer[10] and self-aerated flow[11] calculations. A comparison between data and correlations (Table 4) indicates that the correlation of Wilhelms *et al.*[26] provides the best fitting for these data (Fig. 6). In Fig. 6, the data are compared with two different predictions.

Dissolved oxygen downstream of a hydraulic structure

Results

25. At a weir (Fig. 1), the overall aeration efficiency is

$$E = E_{SA} + E_{HJ} (1 - E_{SA}) \qquad (16)$$

where E_{SA} is the self-aeration efficiency, and E_{HJ} is the efficiency of the hydraulic jump. It should be noted that E_{SA} and E_{HJ} must be taken at the same temperature of reference.

*Table 4. Oxygen transfer at hydraulic jumps**

References (1)	Formula (2)	Remarks (4)
Holler[38]	$r_{20} - 1 = 0{\cdot}0463\ \Delta V^2$	Model experiments: $0{\cdot}61 < \Delta V < 2{\cdot}44$ m/s $277{\cdot}15 < T < 299{\cdot}15K$
Apted and Novak[47]	$r_{15} = 10^{(0{\cdot}24\ \Delta H)}$	Model experiments: $2 < Fr < 8$ $q_w = 0{\cdot}04$ m^2/s
Avery and Novak[48]	$r_{15} - 1 = 0{\cdot}023\left(\frac{q_w}{0{\cdot}0345}\right)^{3/4}\left(\frac{\Delta H}{d}\right)^{4/5}$	Model experiments: $2 < Fr < 9$ $1{\cdot}45E+4 < Re < 7{\cdot}1E+4$ $0{\cdot}013 < d < 0{\cdot}03$ m $287{\cdot}15 < T < 291{\cdot}15K$ $W = 0{\cdot}10$ m
Avery and Novak[40]	$r_{15} - 1 = k'\ Fr^{2{\cdot}1}\ Re^{0{\cdot}75}$ $k' = 1{\cdot}0043E-6$: tap water with 0% $NaNO_2$ $k' = 1{\cdot}244E-6$: tap water with 0·3% $NaNO_2$ $k' = 1{\cdot}5502E-6$: tap water with 0·6% $NaNO_2$	Model experiments: $1{\cdot}45E+4 < Re < 7{\cdot}1E+4$ $\upsilon = 1{\cdot}143E-6$ m^2/s $W = 0{\cdot}10$ m
Wilhelms *et al.*[26]	$r_{15} - 1 = 4{\cdot}924E-8\ Fr^{2{\cdot}106} Re^{1{\cdot}034}$	Model experiments: $1{\cdot}89 < Fr < 9{\cdot}5$ $2{\cdot}4E+4 < Re < 4{\cdot}3E+4$ $W = 0{\cdot}381$ m
Johnson[24]	Empirical fit based on field data from 24 hydraulic structures	Prototype data; works well for deep plunge pools

* d upstream flow depth (m)
Fr upstream Froude number defined as: $Fr = V/\sqrt{gd}$
Re upstream Reynolds number defined as: $Re = Vd/\nu$
r_{15}, r_{20} oxygen deficit ratio at 15°C, 20°C
W channel width (m)
ΔH head loss in the hydraulic jump (m of water)

26. In Fig. 7, field data[1,2] are compared with equation (16) computed using the self-aeration and hydraulic jump calculations described above. The two data sets are compared computations obtained with a single calculation method. The results indicate that the combination of self-aerated flow calculations and hydraulic jump correlation provide a reasonable estimate of the oxygen transfer at weirs and spillways.

Discussion: self-aeration efficiency

27. The Author[6] performed a series of oxygen transfer calculations in self-aerated flows, assuming zero salinity, constant channel slopes ranging from 15° up to 60°, channel lengths between 20 m and 250 m, discharges, from 0·5 m/s² to 50 m/s², roughness heights between 0·1 mm and 10 mm (e.g. concrete channels) and temperatures between 5° and 30°.

28. The analysis of the oxygen transfer computations indicates that the free-surface aeration efficiency is independent of the initial gas content. For discharges larger than 0·5 m²/s, the numerical results suggest that the aeration efficiency can be correlated by

$$E_{SA} = \left(1 - \frac{q_w}{(q_w)_c}\right)^{(15{\cdot}38 - 0{\cdot}0351\,T)\,(\sin\alpha)^{-1/3{\cdot}13}} \qquad (17)$$

where $(q_w)_c$ is the discharge for which the growing boundary layer reaches the free surface at the spillway end, and no self-aeration occurs. The characteristic discharge $(q_w)_c$ can be deduced from Wood's[10] formula

$$(q_w)_c = 0{\cdot}0805\,(L_{spillway})^{1{\cdot}403}\,(\sin\alpha)^{0{\cdot}388}\,k_s^{0{\cdot}0975} \qquad (18)$$

where $L_{spillway}$ is the spillway length, and k_s is the roughness height.

29. In Fig. 8, experimental data[1] for prismatic channels, numerical calculations (§§ 7–22) and equation (17) are compared. The results are encouraging and suggest that equation (17) can provide a first estimate of the self-aeration efficiency. Equation (17) provides E_{SA} as a function of the discharge, slope and roughness height, for a given temperature. It should be noted that equation (17) is an empirical correlation that has been developed for the dissolved oxygen content only.

30. Self-aeration measurements and calculations indicate that: the aeration efficiency increases with the temperature as observed previously;[2,27,28] the aeration decreases when the discharge increases. It must be emphasized that the calculations become inaccurate for flat slopes (i.e. $\alpha < 15$ degrees). For flat channels, little self-aeration occurs and the gas transfer process becomes dominated by turbulent mixing.[29] This process is not discussed in this Paper.

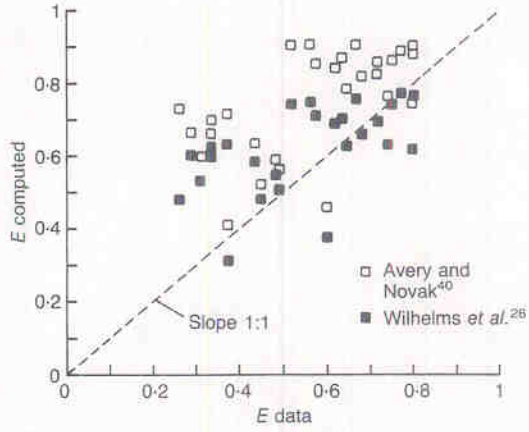

Fig. 6. Oxygen transfer at hydraulic jump on prototype weirs

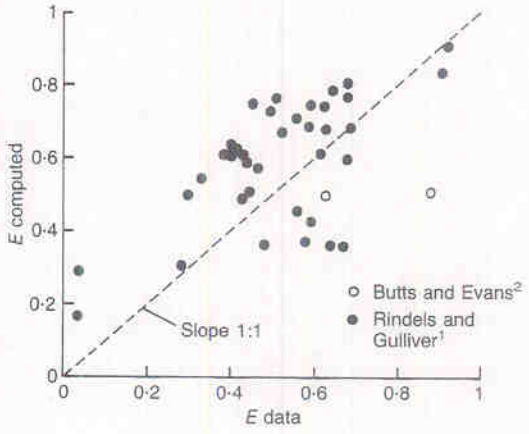

Fig. 7. Overall oxygen transfer at weirs and structures: comparison between calculations and experimental data[1,2]

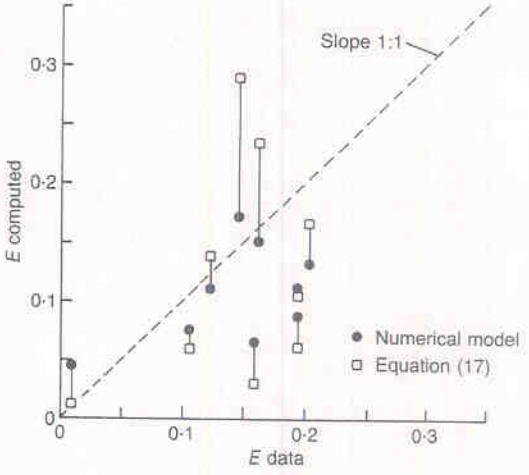

Fig. 8. Free-surface aeration: comparison between numerical model calculations, equation (17) and experimental data for spillway of constant slope

Conclusions

31. Along a chute, the upstream flow is unaerated and little gas transfer takes place. Downstream of the inception point of air entrainment, the presence of air bubbles within the flow increases significantly the interface area and the gas transfer. The characteristics of self-aerated flows can be computed with a simple numerical method. These calculations

provide, at any position, the bubble size distribution and the specific interface area, from which the dissolved gas content can be deduced. For hydraulic jumps, a review of the existing correlation suggests that one formula[26] provides best results for some field data.[1]

32. Self-aeration and hydraulic jump calculations can be combined to predict the aeration efficiency of weirs. The calculations have highlighted that the discharge is a critical parameter in the air–water gas transfer. At low discharges, self-aeration may contribute up to 80–100% of the total gas transfer (equation (17)). For large discharges, there is a critical discharge above which self-aeration does not occur along the spillway, and gas transfer occurs only in the hydraulic jump.

33. It must be emphasized that there is an insufficient number of data available and that the calculations depend greatly on the estimation of the transfer coefficient K_L.

Appendix 1. Bubble breakup in self-aerated flows

34. In self-aerated flows (Fig. 1), observations of bubble diameters (Table 5) indicate that the bubble sizes are larger than the Kolmogorov microscale and smaller than the turbulent macroscale. The length scales of the vortices responsible for breaking up bubbles are close to the bubble size.[30,31] These eddies lie within the inertial range and are isotropic.[30,32] Assuming that the breakup of air bubbles is caused by shear fields over the length of a bubble, the turbulent fluctuation equals: $v'^2 = (\omega\, d_b)^2$ where ω is the vorticity.[33] If the acceleration term dV/dx is small, the vorticity equals: $\omega = dV/dy$. It yields

$$v'^2 \sim \left(\frac{dV}{dy}\, d_b\right)^2 \tag{19}$$

35. Equation (19) implies that the bubble diameter is of the order of magnitude of the Prandtl mixing length.[6] With this approximation, a maximum bubble size in self-aerated flows $(d_b)_c$ is deduced from equation (10)

$$\frac{(d_b)_c}{Y_{90}} \sim \sqrt[3]{\left[72\,\frac{(We)_c}{(We)_*}\left(\frac{y}{Y_{90}}\right)^{5/3}\right]} \tag{20}$$

36. Equation (20) is compared in Fig. 3 with prototype and model data (Table 5). Equation (20) satisfies the common sense that the maximum bubble size increases with the depth as the shear stress decreases.[34] These results are consistent with observations.[15,19,21] Halbronn *et al.*[19] observed 'only extremely fine bubbles' (i.e. $d_b < 1$ mm) near the bottom as described by equation (20) (Fig. 3).

Appendix 2. Definition of an ideal air–water interface

37. Air concentration distributions obtained from model and prototype[15,16,19,23] exhibit continuous curves with respect to the distance normal to the spillway bottom. In the lower flow region, air bubbles

Table 5. Average air bubble size in self-aerated flows: observed values

Experiment (1)	Slope: deg. (2)	q_w: m^2/s (3)	V_{90}: m/s (4)	Y_{90}: m (5)	d_b: mm (6)	Comments (7)
Halbronn *et al.*[19]	14·0	0·12–0·37	4–9	0·04–0·09	1·5—5 (a)	Model $W = 0{\cdot}5$ m; $k_s = 0{\cdot}5$ mm
Thandaveswara[49]	15·4–28	0·062–0·189			0·5–2	Model. $W = 0{\cdot}457$ m; $k_s = 0{\cdot}91$ mm
Aviemore dam spillway[15]	45·0	2·23 and 3·16	19–21·7 19–21·7 20·2 20·2	0·21–0·31 0·21–0·31 0·285 0·285	0·5–3 3–20 0·5–3 3–20	$C < 0{\cdot}5$; prototype; wide channel; $k_s = 1$ mm $0{\cdot}5 < C < 0{\cdot}9$ $y/Y_{90} < 0{\cdot}30$; $C < 0{\cdot}20$ $y/Y_{90} > 0{\cdot}30$; $C > 0{\cdot}20$
Volkart[21]	12·0				1–10 1–6·5 (b)	Air bubbles Water droplets Circular pipe. $D = 0{\cdot}24$ m
Cain and Wood[50]	45·0	2·23–6·7			0·5–3 10–20	Near the invert (c) Next to the free surface (c)
Clyde dam model[16]	52·3	0·20–0·40	12·3–17·8	0·036–0·054	0·3–4	Flow downstream of an aerator $W = 0{\cdot}25$ m; $k_s = 0{\cdot}1$ mm
St Anthony Falls[22]		0·136–0·793			0·7–2·7	$W = 0{\cdot}457$ m; $k_s = 0{\cdot}7$ mm (d)

(a) extremely fine bubbles observed near the bottom
(b) water droplet diameters
(c) based on experiments performed at Aviemore dam[15,37]
(d) based on Straub and Anderson's[23] experiments

Table 6. Definitions of the air–water interface in self-aerated flows

Notation (1)	Definition (2)	References (3)
d_T	Transition depth (i.e. interface depth) where dC/dy is maximum. $0{\cdot}45 < C(y = d_T) < 0{\cdot}65$ for $C_{mean} < 0{\cdot}57$	23, 49, 51
Y_{60}	Air–water interface depth where the air concentration is 60%	19, 52, 53
Y_{90}	Free surface of the homogeneous air–water mixture in which the slip ratio equals unity	10, 11, 16, 34, 54

are surrounded by water; in the upper flow region, water droplets are surrounded by air.[15,19,23,35] Previous studies (Table 6) have defined the air–water interface as a function of the shape of the air concentration profile or for a given air concentration. In the upper flow region, high speed photographs[21,36] showed overturning surface waves and water droplets being projected above the water surface and then falling back. Killen[36] discussed the concept of 'air entrained flows' near the water surface. In any case, experimental works[15,16,37] showed that the air–water flow behaves as a homogeneous mixture below 90% of air concentration.[34] Further, a review of these studies and those presented in Table 6 indicates that: for $C < 40\%$, the air–water flow is characterized by air bubbles and air pockets surrounded by a continuous water phase; for $C > 65\%$, the mixture consists of water droplets flowing in an air flow. In between (i.e. $40\% < C < 65\%$), the flow is an undefinable air–water mixture.

38. As a first approximation the ideal air–water interface can be advantageously defined as the location where the air concentration is 50%. This definition is consistent with the experimental observations reported in Table 6.

References

1. Rindels A. J. and Gulliver J. S. Measurements of oxygen transfer at spillways and overfalls. *St Anthony Falls Hydraulic Laboratory Project Report*. University of Minnesota, Minneapolis MN, 1989, No 266.
2. Butts T. A. and Evans R. L. Small stream channel dam aeration characteristics. *J. Environ. Engng, Am. Soc. Civ. Engrs*, 1983, **109**, No. 3, 555–573.
3. Streeter V. L. and Wylie E. B. *Fluid mechanics*. McGraw-Hill, Singapore, 1981, 1st SI Metric edn.
4. Kawase Y. and Moo-Young M. Correlations for liquid-phase mass transfer coefficients in bubble column reactors with Newtonian and non-Newtonian fluids. *Can. J. Chem. Engng*, 1992, **70**, Feb., 48–54.
5. Higbie R. Rate of absorption of a gas into a still liquid. *Trans. Am. Inst. Chem. Engrs*, 1935, **31**, 365–389.
6. Chanson H. Environmental impact of large water releases in chutes: Oxygen and nitrogen contents due to self-aeration. *Proc. 25th IAHR Congress*, Tokyo, 1993b, **5**, 273–280.
7. Gameson A. L. H. Weirs and the aeration of rivers. *J. Inst. Water Eng. Sc.*, 1957, **11**, 477–490.
8. APHA, AWWA, and WPCF. *Standard methods for the examination of water and wastewater*. American Public Health Association Publication, 1989, 7th edn.
9. Elmore H. L. and West W. F. Effect of water temperature on stream reaeration. *J. Sanitary Engng, Am. Soc. Civ. Engrs*, 1961, **87**, No. SA6, 59–71.
10. Wood I. R. Air water flows. *21st IAHR Congress*, Melbourne, 1985, 18–29.
11. Chanson, H. Self-aerated flows on chutes and spillways. *J. Hydraul. Engng, Am. Soc. Civ. Engrs*, 1993a, **119**, No. 2, 220–243.
12. Keller R. J. and Rastogi A. K. Design chart for predicting critical point on spillways. *J. Hydraul. Div. Am. Soc. Civ. Engrs*, 1977, **103**, HY12, 1417–1429.
13. Chanson H. Flow downstream of an aerator. Aerator spacing. *J. Hydraul. Res.*, 1989, **27**, No. 4, 519–536.
14. Wood I. R. (Kobus H. (ed.)). Air entrainment in high speed flows. *Symp. on Scale Effects in modelling Hydraulic Structures*, IAHR, Esslingen, 1984.
15. Cain P. *Measurements within self-aerated flow on a large spillway*. University of Canterbury, Christchurch, New Zealand, 1978, PhD thesis.
16. Chanson H. *A study of air entrainment and aeration devices on a spillway model*. University of Canterbury, Christchurch, New Zealand, Oct. 1988, Research Report 88-8.
17. Chanson H. *Drag reduction in self-aerated flows. Analogy with dilute polymer solutions and sediment laden flows*. Department of Civil Engineering, University of Queensland, Australia, Oct. 1992, Research Report CE 141.
18. Hinze J. O. Fundamentals of the hydrodynamic mechanism of splitting in dispersion processes. *J. Am. Inst. Chem. Engrs*, 1955, **1**, No. 3, 289–295.
19. Halbronn G., Durand R. and Cohen De Lara G. Air entrainment in steeply sloping flumes. *Proc. 5th IAHR Congr.*, IAHR–ASCE, Minneapolis, 1953, 455–466.
20. Straub L. G. and Lamb O. P. Experimental studies of air entrapment in open-channel flows. *Proc. 5th IAHR Congr.*, IAHR–ASCE, Minneapolis, 1953, 425–437.
21. Volkart P. The mechanism of air bubble entrainment in self-aerated flow. *Int. J. Multiphase Flow*, 1990, **6**, 411–423.
22. Gulliver J. S., Thene J. R. and Rindels A. J. 'Indexing gas transfer in self-aerated flows. *J. Environ. Engng, Am. Soc. Civ. Engrs*, 1990, **116**, No. 3, 503–523; Discussion: 1991, **117**, 866–869.
23. Straub L. G. and Anderson A. G. Experiments on self-aerated flow in open channels. *J. Hydraul. Div. Am. Soc. Civ. Engrs*, 1958, **84**, No. HY7, 1890-1–1890-35.
24. Johnson P. L. Prediction of dissolved gas transfer in spillway and outlet works stilling basin flows.

Proc. 1st Int. Symp. on Gas Transfer at Water Surfaces, Gas Transfer at Water Surfaces, 1984, (Brutsaert W. and Jirka G. H. (eds)) 605–612.
25. RINDELS A. J. and GULLIVER J. S. Air–water oxygen transfer at spillways and hydraulic jumps. *Proc. Water Forum '86: World Water Issues in Evolution*, American Society of Civil Engineers, New York, 1986, 1041–1048.
26. WILHELMS S. C. *et al. Gas transfer in hydraulic jumps*. US Army Engineer Waterways Experiment Station, CE, Vicksburg, Mississippi, 1981, Technical Report E-81-10.
27. GAMESON A. L. H., VANDYKE K. G. and OGDEN C. G. The effect of temperature on aeration at weirs. *Water & Water Engng*, 1958, Nov., 489–492.
28. DEPARTMENT OF THE ENVIRONMENT. Aeration at weirs. *Notes on Water Pollution*, No. 61, Water Research Laboratory, Stevenage, 1973.
29. GULLIVER J. S. and HALVERSON M. J. Air–water gas transfer in open channels. *Water Resources Res.*, 1989, **25**, No. 8, 1783–1793.
30. SEVIK M. and PARK S. H. The splitting of drops and bubbles by turbulent fluid flow. *J. Fluids Engng*, 1973, **95**, 53–60.
31. KUMAR S., NIKITOPOULOS D. N. and MICHAELIDES E. E. Effect of bubbles on the turbulence near the exit of a liquid jet. *Experiments in Fluids*, 1989, **7**, 487–494.
32. EVANS G. M., JAMESON G. J. and ATKINSON B. W. Prediction of the bubble size generated by a plunging liquid jet bubble column. *Chem. Eng. Sc.*, 1992, **47**, No. 13/14, 3265–3272.
33. LEWIS D. A. and DAVIDSON J. F. Bubble splitting in shear flow. *Trans. Inst. Chem. Engrs*, 1982, **60**, 283–291.
34. WOOD I. R. Air entrainment in free-surface flows. *IAHR hydraulic structures design manual No. 4*. Hydraulic Design Considerations, Balkema Publications, Rotterdam, 1991.
35. STRAUB L. G., KILLEN J. M. and LAMB O. P. Velocity measurements of air–water mixtures. *Trans. Am. Soc. Civ. Engrs*, 1954, **119**, 207–220.
36. KILLEN J. M. *The surface characteristics of self-aerated flow in steep channels*. University of Minnesota, Minneapolis, 1968, PhD thesis.
37. KELLER R. J. *Field measurement of self-aerated high speed open channel flow*. Department of Civil Engineering, University of Canterbury, New Zealand, 1972, PhD thesis.
38. HOLLER A. G. The mechanism describing oxygen transfer from the atmosphere to discharge through hydraulic structures. *Proc. 14th IAHR Congr.*, Paris, 1971, **1**, 372–382.
39. FOREY E. G. Reaeration and velocity prediction for small streams. *J. Environ. Engng*, 1976, **102**, No. EE5, 937–952.
40. AVERY S. T. and NOVAK P. Oxygen transfer at hydraulic structures. *J. Hydraul. Div. Am. Soc. Civ. Engrs*, 1978, **104**, No. HY11, 1521–1540.
41. NAKASONE H. Study of aeration at weirs and cascades. *J. Environ. Engng, Am. Soc. Civ. Engrs*, 1987, **113**, No. 1, 64–81.
42. RAILSBACK S. F. *et al.* Aeration at Ohio River Basin navigation dams. *J. Environ. Engng, Am. Soc. Civ. Engrs*, 1990, **116**, No. 2, 361–375.
43. RINDELS A. J. and GULLIVER J. S. (WILHELMS S. C. and GULLIVER J. S. (Eds)). Oxygen transfer at spillways. *Proc. 2nd Int. Symp. on Gas Transfer at Water Surfaces: Air–Water Mass Transfer*, ASCE Publications, Minneapolis, 1990, 524–533.
44. DANIIL E. I. and GULLIVER J. Temperature dependence of liquid film coefficient for gas transfer. *J. Environ. Engng*, 1988, **114**, No. 5, 1224–1229.
45. DANIIL E. I., GULLIVER J. and THENE J. R. Water-quality assessment for hydropower. *J. Environ. Engng, Am. Soc. Civ. Engrs*, 1991, **117**, No. 2, 179–193.
46. KILLEN J. M. Maximum stable bubble size and associated noise spectra in a turbulent boundary layer. *Proc. Cavitation and Polyphase Flow Forum*, American Society of Mechanical Engineers, 1982, 1–3.
47. APTED R. W. and NOVAK P. Oxygen uptake at weirs. *Proc. 15th IAHR Congr.*, Istanbul, 1973, **1**, 177–186.
48. AVERY S. T. and NOVAK P. Oxygen uptake in hydraulic jumps and at overfalls. *Proc. 16th IAHR Congr.*, Sao Paulo, 1975, 329–337.
49. THANDAVESWARA B. S. *Self-aerated flow characteristics in developing zones and in hydraulic jumps*. Department of Civil Engineering, Indian Institute of Science, Bangalore, 1974, PhD thesis.
50. CAIN P. and WOOD I. R. Instrumentation for aerated flow on spillways. *J. Hydraul. Div. Am. Soc. Civ. Engrs*, 1981a, **107**, HY11, Nov., 1407–1424.
54. CAIN P. and WOOD I. R. Measurements of self-aerated flow on a spillway. *J. Hydraul. Div. Am. Soc. Civ. Engrs*, 1981b, **107**, HY11, 1425–1444.
51. RAO N. S. L. and KOBUS H. E. Characteristics of self-aerated free-surface flows. *Water and Waste Water/Current Research and Practice*, 1971, **10**, Eric Schmidt Verlag, Berlin.
52. PAN S. B. *et al.* Self-aeration capacity of a water jet over an aeration ramp. *Shuili Xuebao* (J. Hydraul. Engng), Beijing, 1980, No. 5, 13–22 (in Chinese). (USBR translation No. 1868, Book No. 12 455, paper No. 2.)
53. YUAN MINGSHUN. Calculation of 2-D air concentration distribution downstream of an aerator. *Shuili Xuebao* (J. Hydraul. Engng), Beijing, 1991, No. 12, 10–17 (in Chinese).